PROBLEMS OF CREATING MATERIALS AND FILM STRUCTURES BASED ON FERRITS FOR SPINTRONICS DEVICES

Valery A. Ketsko, Maria N. Smirnova, Maria A. Kopieva, Evgeny N. Beresnev

Kurnakov Institute of General and Inorganic Chemistry, Russian Academy of Sciences, http://igic.ras.ru
Moscow 119991, Russian Federation

ketsko@igic.ras.ru, smirnova_macha1989@mail.ru, mkopieva@mail.ru, benko@igic.ras.ru

Abstract. **The review presents the main directions of the search for materials and film structures based on them for spintronics devices, provides data on materials for these purposes available in the literature. The problems that need to be solved when creating spintronics structures are analyzed. A new method for the synthesis of ferrite films on semiconductor substrates without elastic stresses and unwanted interactions of components at the interface is presented. A method for the synthesis of powdered ferrites, based on burning the gel, characterized by phase homogeneity and dimensional unimodality, which makes it possible to use the material as a target for the synthesis of films, is considered. The prospects for the practical use of submicron films of ferrite garnets with a SiO_2 buffer layer on Si with a Hilbert damping parameter $\alpha \approx 10^{-3}$, which can be used in spin-wave device structures on silicon substrates, are considered.**

Keywords: **spintronics, ferrites, homogeneous powders, new method for creating film structures, properties of structures**

UDC 546.027

Bibliography - 46 references *Received November 1, 2018; adopted December 10, 2018*

RENSIT, 2018, 10(3):381-394 **DOI: 10.17725/rensit.2018.10.381**

Contents

1. INTRODUCTION

It is known that the increase in the speed of processing and transmitting information in modern microelectronics devices is approaching the limit due to the fundamental physical limitations on the further reduction of the size of active elements. In this regard, in order to expand the capabilities of electronic devices, it is necessary to search for and create new technological approaches that would ensure further progress in this field of science and technology.

Using, along with the charge of an electron, its spin will allow in the future to create instrument film devices that are integrally controlled by magnetic and electric fields, which can be: spin field-effect transistors, ultrafast frequency tuning filters, coatings and screens absorbing electromagnetic radiation in a wide wavelength range , as well as matching devices in antenna systems and receiving modules of the microwave range, tunable delay lines, noise suppressors, etc. These structures can be applied in satellite communications and radiolocation systems, cellular telephony, digital television systems, etc.

An important characteristic of new electronic devices in terms of future technologies is their energy efficiency. When using them, there is no need for high current

densities, energy losses are sharply reduced and the signal transmission rate increases.

2. BASIC DIRECTIONS OF SEARCH OF MATERIALS AND FILM STRUCTURES OF SPINTTRONICS

At present, the search for new materials and film heterostructures with both semiconductor and magnetic characteristics at temperatures above room temperature is conducted in two main directions [1-3].

The first direction is connected with the creation of a "ferromagnet-semiconductor" film composite structure, obtained by sequential layer spraying of the structure components. Such a path is quite attractive due to the variety of existing magnetic and semiconductor materials, which can be combined to make a directed search for structures with the necessary properties. Such a hybrid structure should be considered as exchange-related. It should be noted that in this case the contact of a ferromagnet (FM) with a semiconductor (PP) is accompanied by two effects: the Hall effect in a semiconductor under the action of the magnetic field of the ferromagnet, and the formation of a Schottky barrier due to the distortion of the band structure [1, 4], which is accompanied by the accumulation near the film – substrate interface is a significant number of charge carriers. In this case, a strong exchange interaction near the interface region between charge carriers in PP and magnetic atoms in FM can lead to the appearance of a unified spin system. The disadvantage of this approach is a small spin relaxation time, which limits the use of such structures.

As an example, we can cite a number of works in which the results of studies of FM films on zinc oxide substrates are presented. Thus, in the works, the authors, using various methods of synthesis (sol-gel [5], reactive sputtering [6], laser evaporation [7]) obtained ferromagnetic (T_C above 350 K) films ($0 < x < 0.25$ [5], $0.035 < x < 0.115$ [6], $x < 0.4$ [7]), in which there were no cobalt clusters. In [8], films ($x = 0.05$-0.25) deposited on a sapphire substrate by the method of pulsed laser evaporation were ferromagnetic and retained magnetic ordering at temperatures above room temperature.

At the same time, other authors argue that solid solutions with wurtzite structure are predominantly paramagnetic [9-11]. At the same time, in films ($x = 0.25$) obtained by the method of pulsed laser decomposition [9], ferromagnetism is caused by the presence of cobalt clusters, and in polycrystals ($x = 0.05$, 0.1 and 0.15) synthesized by the solid phase method [10], and in single crystals, grown by the melt technique [11], due to the presence of impurities.

In some papers, information is given on the existence of ferromagnetism (T_C above 300 K) in 3*d*-doped wide-gap semiconductors GaN [4], AlN [12], ZnO [13-16], TiO_2 [17], SnO_2 [18-21].

In a number of works [21-24], the occurrence of ferromagnetism in undoped 3*d*-elements SnO_2 has been reported. It is assumed that this effect may occur either with a large number of defects in the crystal lattice, or its appearance is associated with the size factor.

The authors of [25] investigated phase equilibria in the Co-Zn-O system and showed that in solid solutions $Zn_{1-X}Co_XO_{1+\delta}$, where $x \leq 0.2$, there is only antiferromagnetic ordering, and the manifestation of ferromagnetism in ceramics is most likely associated with the violation of homogeneity or the presence of impurities.

The second direction of the search is based on the creation of homogeneous materials with both semiconductor and magnetic properties, which must satisfy three basic criteria: the simplicity and reliability of synthesis

methods, the possibility of including products derived from these materials into standard semiconductor circuits; preservation of the structure and physicochemical properties of the original semiconductor arrays in the obtained magnetic semiconductor materials without deterioration of their functional characteristics; preservation of the magnetic orientation in semiconductors with n- and p-mobile charge carriers at temperatures above room temperature.

The first open ferromagnetic semiconductor is europium monoxide EuO [26]. Ferromagnetic ordering in EuO and its semiconductor conductivity is associated primarily with the unusual electronic structure of the doubly charged europium ion. Being in the lowest oxidation state for rare-earth metals, Eu^{2+} is characterized by the maximum possible number of unpaired electrons at the 4*f*-electronic level. This provides ferromagnetism with a colossal atomic magnetic moment (7 μB). At the same time, it should be noted that the creation of heterostructures for microelectronic devices based on EuO is difficult due to the low Curie temperature (69.4 K) and the instability of the material in air. In [3], it is said that TC can be enhanced by dissolving samarium monoxide SmO or ytterbium YbO in EuO. Thus, the T_S was increased to 130 K. However, the authors could not significantly raise the Curie temperature due to the fact that the solubility of the oxides SmO and YbO was not high enough (for example, for SmO it was 14 mol%). In addition, solid solutions of $Eu_{1-x}Sm_xO$ or $Eu_{1-X}Yb_XO$, as well as EuO, turned out to be metastable. It should be noted that the functional characteristics of EuO depend on oxygen nonstoichiometry. At the same time, despite the indicated drawbacks, the work on obtaining EuO-based heterostructures continues to this day.

In [28], the authors synthesized EuO – Fe (Co) composites, including in the form of thin films, whose Curie temperatures corresponded to the indicated transition ferromagnetic metals, while the composites themselves remained semiconductors with a band gap $E_g \approx 0.75$ eV.

High Curie temperatures were found in chalcogenide ferromagnetic semiconductors with a spinel structure with the general formula AB_2C_4 (where A is Cd, Hg. Zn, Cu; B is Cr, Fe; C is S, Se, Te) [29]. However, it has not yet been possible to obtain film structures in such materials.

Based on the principles of isovalent substitution of cations in the structure, a solid solution $Ga_{1-x}Mn_xAs$ (where x is up to 5%) was obtained, which had a higher Curie temperature of 170 K compared to EuO [3]. Such substances, which are characterized by a disordered distribution of impurity magnetic ions in the crystal structure, are called diluted magnetic semiconductors – DMS (diluted magnetic semiconductors).

As follows from a brief analysis of the presented results, the range of materials that would satisfy the necessary criteria for their use in spintronic devices is extremely limited. At the same time, recently, the number of publications related to the synthesis and research of materials and film structures based on ferrites with a spinel and garnet structure, which can be used in spintronics devices, has significantly increased [30-32].

3. MAGNETIC SEMICONDUCTOR MATERIALS BASED ON FERRITES

Interest in the creation of electronic devices containing ferrite films on semiconductor substrates increased significantly after the discovery of $Mg(Fe_{0.8}Ga_{0.2})_2O_4$ magnetic semiconductors in the Mg-Fe-Ga-O system [3].

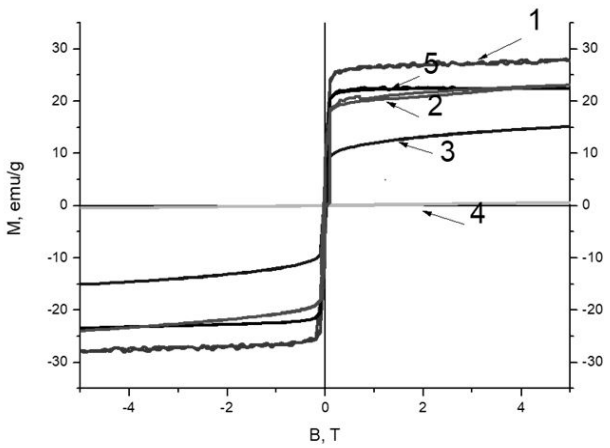

Fig. 1. *Field dependences of the specific magnetization solid solution the $Mg(Fe_{1-x}Ga_x)_2O_4$ at 300 K: 1- $Mg(Fe_{0.8}Ga_{0.2})_2O_4$, 2 - $Mg(Fe_{0.7}Ga_{0.3})_2O_4$, 3 - $Mg(Fe_{0.65}Ga_{0.35})_2O_4$, 4 - $Mg(Fe_{0.2}Ga_{0.8})_2O_4$, 5 - $MgFe_2O_4$.*

As a result of a detailed study of the Mg-Fe-Ga-O system, the authors found that the most optimal combination of functional properties is a solid solution of the composition $Mg(Fe_{0.8}Ga_{0.2})_2O_4$. This material is characterized by Curie temperature (T_C) ~ 450 K, saturation magnetization (M_S) ~ 28 A · m^2 · kg^{-1}, specific electrical conductivity ~ 10^{-8} S/m, band gap ΔE ~ 1.9 eV.

In **Fig. 1** and **Fig. 2** presents the results of studies of the functional characteristics of the $Mg(Fe_{1-x}Ga_x)_2O_4$ solid solution at 300 K.

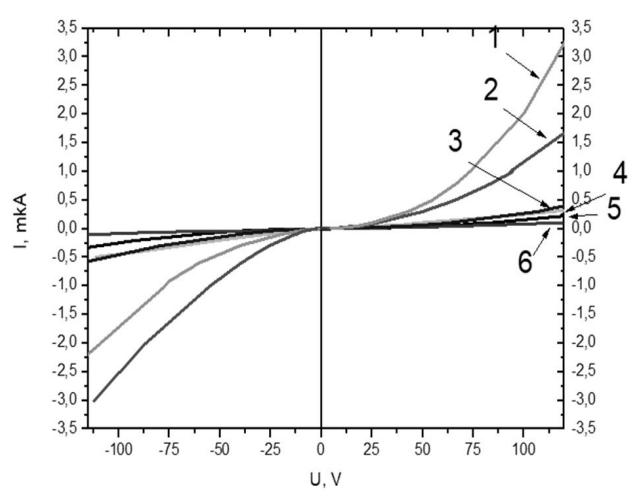

Fig. 2. *Current-voltage characteristics of the solid solution $Mg(Fe_{1-x}Ga_x)_2O_4$ at 300 K: 1- $Mg(Fe_{0.8}Ga_{0.2})_2O_4$, 2 - $Mg(Fe_{0.7}Ga_{0.3})_2O_4$, 3 - $Mg(Fe_{0.65}Ga_{0.35})_2O_4$, 4 - $Mg(Fe_{0.2}Ga_{0.8})_2O_4$, 5 - $MgFe_2O_4$, 6- $MgGa_2O_4$.*

As can be seen from Fig. 1, the magnitude of specific magnetization (MS) reaches saturation only for $Mg(Fe_{0.8}Ga_{0.2})_2O_4$ and $MgFe_2O_4$ at values of the applied external magnetic field of 0.1–0.3 *T*. In this case, the magnitude of M_S in $Mg(Fe_{0.8}Ga_{0.2})_2O_4$ (M_S = 28) is higher compared to M_S of magnesium ferrite $MgFe_2O_4$ (M_S = 23). At the same time, in $Mg(Fe_{0.7}Ga_{0.3})_2O_4$ and $Mg(Fe_{0.65}Ga_{0.35})_2O_4$, M_S does not reach saturation values even in external fields up to 4*T*, which indicates magnetic inhomogeneity of materials.

However, a significant disadvantage of both $Mg(Fe_{0.8}Ga_{0.2})_2O_4$ and ferrites in general is the high (850–950°*C*) crystallization temperature, as well as the significant mismatch of the crystallographic parameters of their lattices with commercial semiconductors such as Si, GaN and GaAs. At these temperatures, elastic stresses arise in the heterostructures, initiated by the processes of crystallization of the films, and undesirable interactions of the components at the interface occur, which leads to a significant decrease in their functional characteristics.

As an example in **Fig. 3** shows the results of study the cross section of the $Mg(Fe_{0.8}Ga_{0.2})_2O_4$/Si heterostructure after

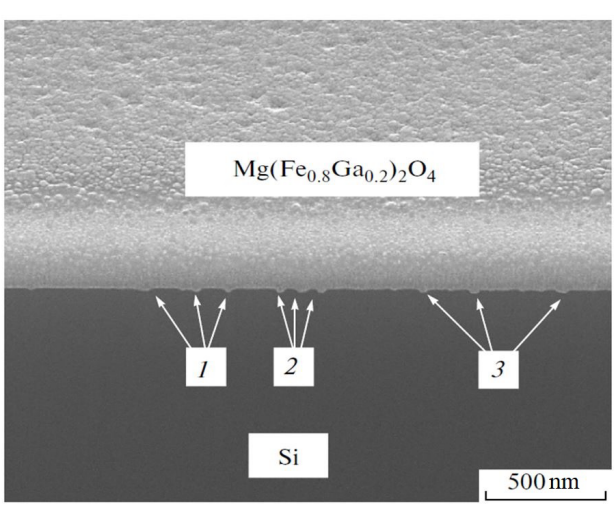

Fig. 3. *SEM imaging the cross section of the $Mg(Fe_{0.8}Ga_{0.2})_2O_4$/Si heterostructure after crystallization at 1173 K for 10 min (Figures 1, 2, 3 show the areas of interaction $Mg(Fe_{0.8}Ga_{0.2})_2O_4$ with Si).*

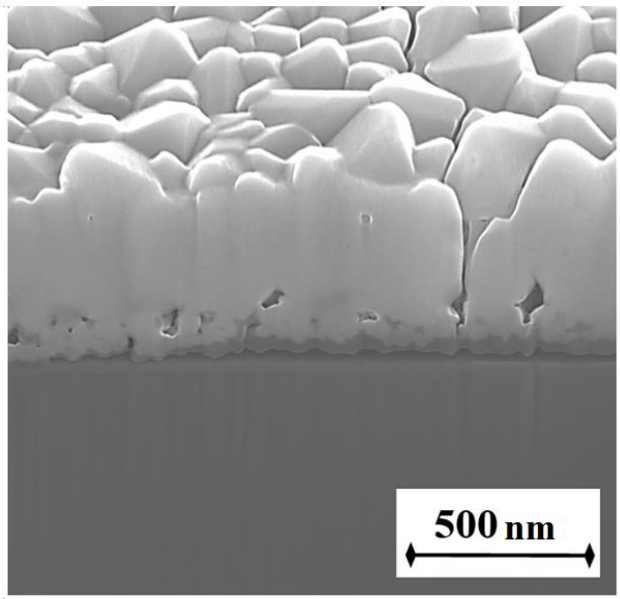

Fig. 4. *SEM imaging the cross section of the $Mg(Fe_{0.8}Ga_{0.2})_2O_4/Si$ heterostructure after crystallization at 1173 K for 30 min.*

the film crystallizes at 1173 K for 10 min. It can be seen from the figure that an intensive interaction occurs at the film/substrate interface, leading to a decrease in the primarily magnetic characteristics of the substituted ferrite.

In **Fig. 4** shows the SEM image of the cross section of the $Mg(Fe_{0.8}Ga_{0.2})_2O_4/Si$ heterostructure after crystallization at 1173 K for 30 min. It can be seen that the film contains numerous defects, local delaminations from the substrate are also seen.

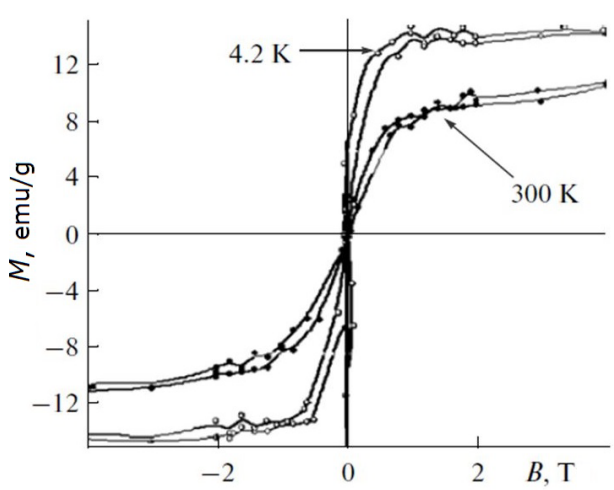

Fig. 5. *Magnetization curves of $Mg(Fe_{0.8}Ga_{0.2})_2O_4$ film on Si with a thickness of 200 nm after its crystallization at 800 K for 30 min* [6].

In **Fig. 5** shows the results of studies of the magnetization curves of the $Mg(Fe_{0.8}Ga_{0.2})_2O_4$ film on Si with a thickness of 200 nm after its crystallization at 800 K for 30 min. It can be seen from the figure that M_S is much less than the analogous value for powdered $Mg(Fe_{0.8}Ga_{0.2})_2O_4$ and does not reach saturation at room temperature in an external magnetic field exceeding 4*T*.

4. A NEW WAY OF OBTAINING FERRITE FILMS ON SEMICONDUCTOR SUBSTRATES

The authors of [33] proposed a method for obtaining microelectronic-quality ferrite films on semiconductor and dielectric substrates without elastic stresses and undesirable interactions of components at the interface. The film structures were obtained by ion-beam sputtering, which allows the transfer of the metal oxide target material to the substrate without changing the cationic composition, ensuring the density of the submicron thickness layer close to the density of the bulk target material, and achieving high adhesion of the deposited layer due to the presence of a high-energy component in the flow adatoms.

For an effective implementation of this method, they applied an integrated approach, which consists in the fact that a method of synthesizing a target material was originally developed, which allows minimizing surface and bulk film defects in the process of its creation, to obtain a uniform thickness and area while ensuring the chemical stability of the interface film/substrate. Then, at the second stage, when creating the film structures, the original idea of the film crystallization process was implemented without heating the substrate.

Note that in most of the works, the quality (phase homogeneity, dimensional unimodality, etc.) of the target material

for the synthesis of films is not given due attention. However, it is this factor that can have a significant effect on the quality of the heterostructures obtained.

To achieve this goal, a method for the synthesis of powdered ferrites was developed, which uses gel burning [34]. The method is based on heat treatment of mixtures containing nitrates of the respective metals and "organic fuel", which must meet certain requirements. First, to form complex compounds with metal salts, which contributes to increasing the solubility of the starting components and prevents precipitation upon evaporation of water. As a result, a uniform distribution of ions in the gel precursor is achieved, the heat treatment of which leads to the formation of a single-phase highly dispersed powdered oxide. Secondly, the organic component of the reaction mixture should generate enough heat to burn/smolder the gel in a self-sustaining mode, which, in turn, eliminates the subsequent high-temperature annealing in order to crystallize the final product. The choice of an effective "organic fuel" took into account these requirements, as well as the individual characteristics of the objects of study.

Let us consider in more detail the process of synthesizing a homogeneous powder that is unimodal in particle size $Mg(Fe_{0.8}Ga_{0.2})_2O_4$ powder by burning a gel using glycine as an "organic fuel" and its mixture with hexamine. Due to its symmetry, the glycine molecule can serve as a bidentate ligand for divalent and trivalent *d*-metals, which contributes to the homogenization of the gel precursor, and, as a consequence, the phase and dimensional uniformity of the final powdered material. The second component of the fuel mixture - hexamine, has attractive calorific properties (calorific value of 4215 kJ/mol), which ensures the initiation of gel burning and the flow of this process in a self-sustaining mode.

Note that the initial solution of metal nitrates was prepared by dissolving metallic magnesium, gallium and carbonyl iron. In a molar ratio of 1:0.4:1.6 in diluted (1:3) nitric acid. Then a mixture of glycine ($H_2N–CH_2–C(O)OH$) and hexamine ($C_6H_{12}N_4$) were added to the solution.

The resulting solutions were evaporated in the reactor with stirring at ~ 100°*C* to the state of gels. At a temperature of > 100°*C*, an intense combustion reaction began (**Fig. 6**). At temperatures of ~ 135-165°*C* (Fig. 6), a sharp mass loss was observed, accompanied by a significant exothermic effect (DSC curve, Fig. 6). It is associated with burning gels.

It is obvious that the actual temperature of combustion of the samples is significantly higher than the specified temperature range. In this regard, the authors of [34] developed a calculation method based on the DSC results to determine the temperature of burning gels. As a result, it turned out that the real temperature of short-term burning is 1040°*C*. At the same time, in the literature, as a rule, only the adiabatic combustion temperature of the samples is indicated, which is several thousand degrees.

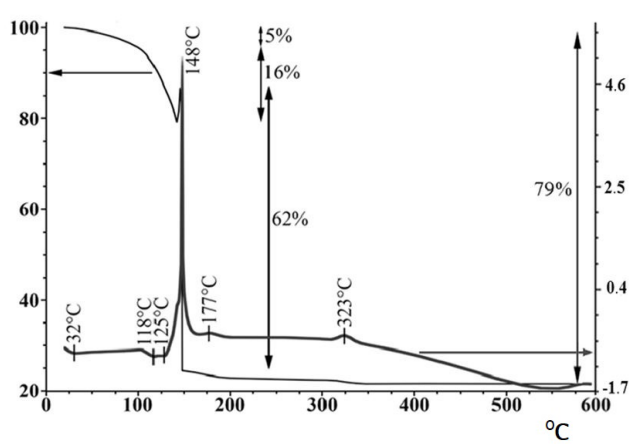

Fig. 6. *TGA-DSC of gel (air flow).*

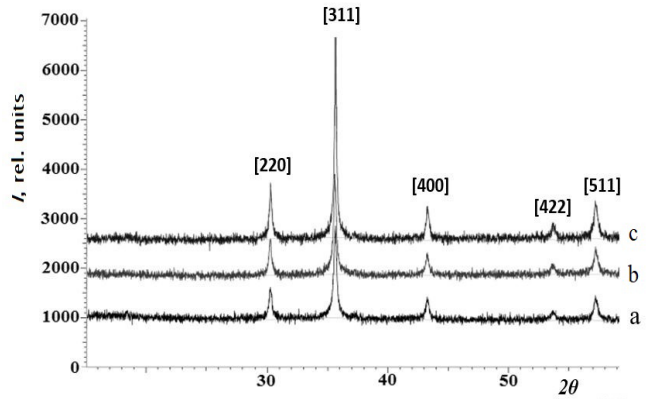

Fig. 7. *XRD patterns of $Mg(Fe_{0.8}Ga_{0.2})_2O_4$ powder: a - after synthesis; b - annealing at 600°C; c - annealing at 700°C.*

On X-ray diffractograms of the powders (**Fig. 7**a), after burning and cooling, the reflections of crystalline $Mg(Fe_{0.8}Ga_{0.2})_2O_4$ were recorded. Further heat treatment at 600°*C* and 700°*C* (Fig. 7b, c) contributes to an increase in the degree of crystallinity of the powder and allows one to obtain a single-phase, nano-sized powder with a relative unimodality of particle size distribution without carbon-containing impurities.

Targets for film production were prepared from the synthesized powders.

In this case, the synthesis of ferrite films took place in several stages. Initially, a layer of ferrite from 10 to 20 nm thick was deposited with an ion beam method of oxygen ions with an energy of 1500 to 1600 eV and a beam current density of 0.1 to 0.25 mA/cm^2. The interval of thicknesses was chosen from the following considerations: when the film thickness is less than 10 nm, the magnetic properties of the films after crystallization practically do not appear, and when the layer thickness is more than 20 nm, it is necessary to increase the crystallization temperature of the film.

Then, in the quasi-pulse mode, ferrites crystallized. The speed (150–200°*C*/min) and the exposure time (700–720°*C* for 2–3 min) of the reactor were selected so that the substrate did not heat up during the crystallization of

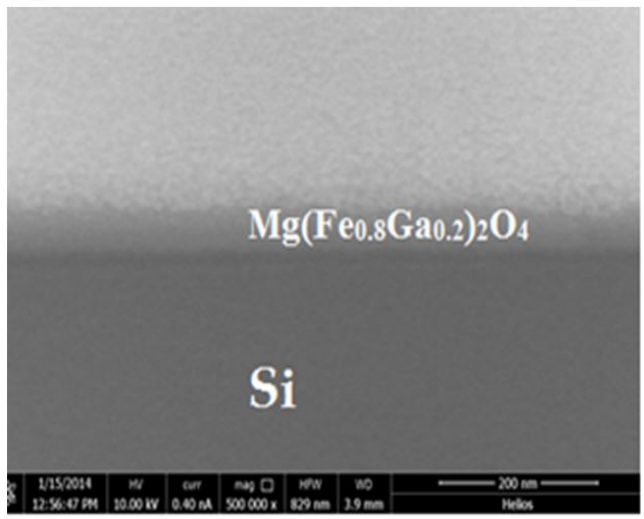

Fig. 8. *SEM image the cross section of $Mg(Fe_{0.8}Ga_{0.2})_2O_4/Si$ heterostructure after crystallization in the quasi-pulse mode.*

the film. After rapid cooling of the reactor, the film was thinned to a thickness of ~ 2 nanometers. As a result of such operations, a ferrite film containing numerous defects (see Fig. 4), formed as a result of its crystallization, was removed.

Next, re-deposition of the film on the germinal crystal layer of ferrite was performed. Thus, a quasi-epitaxial growth of the ferrite film took place, and its subsequent crystallization in the quasi-pulse mode was not accompanied by the formation of defects.

In **Fig. 8** shows the SEM image of the cross section of the $Mg(Fe_{0.8}Ga_{0.2})_2O_4/Si$ heterostructure after quasi-pulse crystallization. It is seen that the interface border is smooth, and there are no defects in the film itself.

In **Fig. 9** shows the SEM images of the surface of the $Mg(Fe_{0.8}Ga_{0.2})_2O_4$ film on the

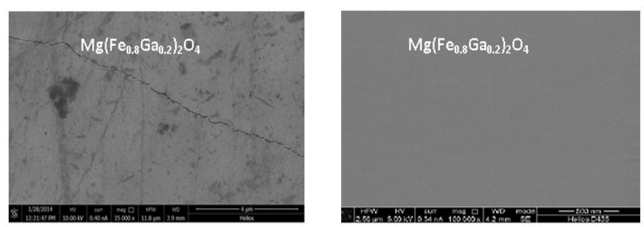

Fig. 9. *SEM images of the surface of the $Mg(Fe_{0.8}Ga_{0.2})_2O_4$ film on the Si substrate after its crystallization in the isothermal (left) and quasi-pulse (right) modes.*

silicon substrate after its crystallization by the isothermal method (left) and in the quasi-pulse mode (right).

It can be seen from the figure that the $Mg(Fe_{0.8}Ga_{0.2})_2O_4$ surface after crystallization in the isothermal mode consists of numerous defects and cracks over the entire film area, and vice versa, the $Mg(Fe_{0.8}Ga_{0.2})_2O_4$ surface remains nano-sized after quasi-pulse crystallization.

It should be noted that the proposed method of creating film structures is quite complex in execution. Its implementation is possible only with the availability of appropriate high-tech sputtering equipment and personnel with high qualifications.

In some cases, when creating film structures, it is possible to use another approach - the use of barrier layers at the interface, which will interfere with the processes of interaction of components during the crystallization of films. At the same time, the question remains whether the composition of the buffer layer affects the functional properties of the structures obtained. The physical properties of film structures were analyzed by the example of films of yttrium iron garnet (YIG, $Y_3Fe_5O_{12}$) on Si with buffer layers of SiO_2 and AlO_x [35].

5. FILM STRUCTURES OF $Y_3Fe_5O_{12}$ ON Si

It is known that epitaxial $Y_3Fe_5O_{12}$ films of micron thickness are usually grown by the method of liquid-phase epitaxy (LPE) on gallium-gadolinium garnet (GGG) substrates due to the small lattice mismatch ≈ 0.06%. At the same time, $Y_3Fe_5O_{12}$ films on silicon or quartz substrates are characterized by higher values of the Hilbert attenuation parameter ≈ 10^{-2} [36], which is caused by the mismatch of the crystal lattices and the temperature expansion coefficients of $Y_3Fe_5O_{12}$ and Si, which excludes their epitaxial growth. However, if we separate the processes of precipitation and crystallization of $Y_3Fe_5O_{12}$, and form a buffer layer on the Si surface in the form of a thin film of SiO_2 or AlO_x, which will prevent third-party chemical reactions during annealing, but at the same time provide high adhesion of the deposited layer to the surface, then we can expect high quality polycrystalline ferrite garnet films. In this case, at the deposition stage, diffusion exchange will be excluded between the substrate, which is perfect in structure and the substrate and film of the material being crystallized, and the role of diffusion processes in the crystallization of the film will be leveled by the high density of the material being deposited.

In **Fig. 10** shows the appearance of the surface of the YIG film in the composition of the $Y_3Fe_5O_{12}$ (260nm)/AlO_x/SiO_x/Si (100) heterostructure (Fig. 10*a*), its cross section (Fig. 10*b*) and its elemental composition (Fig. 10*c*).

From Fig. 10 that the $Y_3Fe_5O_{12}$ film is characterized by the presence of large and

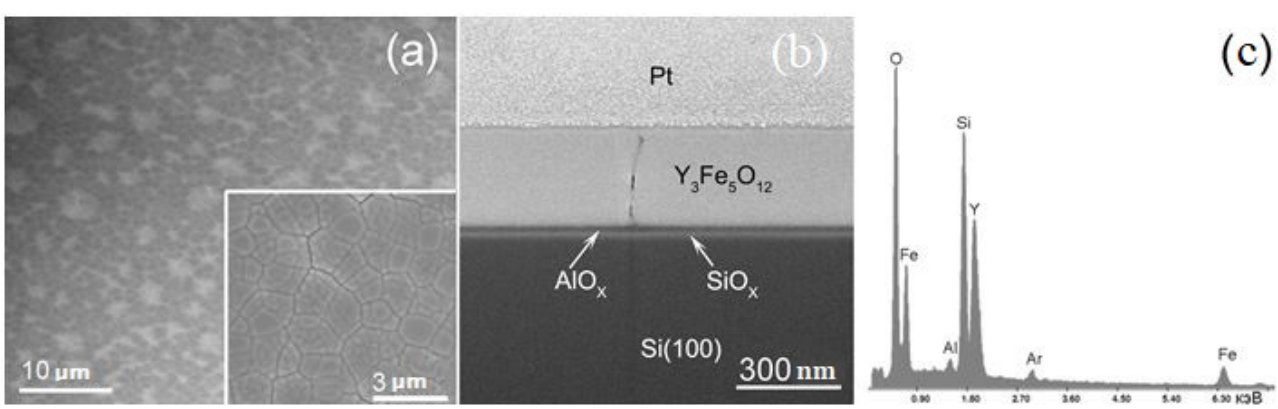

Fig. 10. *SEM image of the surface of the $Y_3Fe_5O_{12}$/AlO_x/SiO_x/Si(100) film heterostructure (Fig. 10a, inset shows a section of the surface with a high resolution).*

small fracture meshes. The characteristic dimensions of large grids of cracks are up to 2 μm, and small ones that are contained inside large ones do not exceed 0.3 μm, which correlates with the thickness of the $Y_3Fe_5O_{12}$film (about 0.3). In this case, the $Y_3Fe_5O_{12}$ film is polycrystalline and consists of single-crystal blocks with characteristic sizes up to 0.3 microns. The interface areas of the grain boundaries, especially when the boundaries of large and small areas coincide, are enriched with defects, which is reflected in the contrast in the appearance of the surface (Fig. 10*a,b*). The fine mesh of cracks does not grow through the entire thickness of the $Y_3Fe_5O_{12}$ film, and the large one extends up to the buffer layer (Fig. 10*b*). It can be seen that the interfaces in the $Y_3Fe_5O_{12}$ (260nm)/AlO_x/SiO_x/Si (100) heterostructure are solid, clear and plane-parallel. In this case, no violations that could be caused by intense interactions with the buffer layer and the substrate are recorded. The elemental composition of the heterostructure (Fig. 10*c*) contains only elements corresponding to the composition $Y_3Fe_5O_{12}/AlO_x/SiO_x$/Si (100). Similar results were obtained for heterostructures with the composition $Y_3Fe_5O_{12}/SiO_2$/Si (111). It should be noted that the formation of cracked grids is also fixed for films of ferrite garnets obtained by the method of magnetron sputtering on Si or quartz substrates [38, 39].

In **Fig. 11** shows X-ray diffraction patterns of film heterostructures $Y_3Fe_5O_{12}$(260nm)/AlO_x(40nm)/SiO_x(10nm)/Si (100) (Fig. 11, curve 1) and $Y_3Fe_5O_{12}$(260nm)/SiO_2(800nm)/Si (111) (Fig. 11, curve 2). For $Y_3Fe_5O_{12}$ films with a thickness of about 200 nm, diffraction patterns identify narrow reflexes of high intensity, which are related to the cubic symmetry of the space group (230) [40]. In this case, the lattice constant of submicron films was about 1.2378 nm, which is somewhat larger

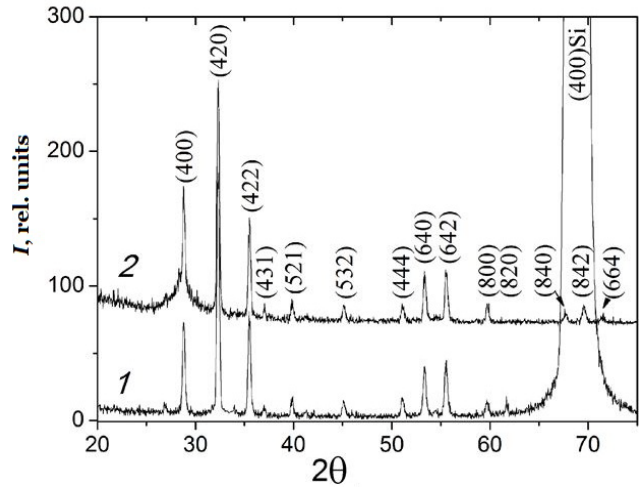

Fig. 11. *X-ray diffraction patterns of typical heterostructures $Y_3Fe_5O_{12}$(200нм)/AlO_x(40нм)/SiO_x(10нм)/Si (100) (Fig. 11, curve 1) and $Y_3Fe_5O_{12}$ (200nm)/SiO_2 (800nm)/Si (111) (Fig. 11, curve 2).*

than that of a bulk YIG single crystal (1.2376 nm [41]). One can see a good agreement of the X-ray diffraction spectra of both samples. In the case of a relatively thick thermally grown layer of SiO_2 (Fig. 11, curve 2), the substrate is completely shielded from X-rays, but this does not lead to a significant deformation of the diffractogram reflections. This is evidence in favor of the non-diffusion mechanism of crystallization of the samples under study. It should also be noted that in films of ferrite garnets obtained by the method of ion-beam sputtering-deposition, the lattice constant always turns out to be greater than the value characteristic of bulk single crystals. The reason for this can be either the intrinsic defect structure of the YIG films, which forms as the crystallization progresses, and the adhesive, rather than epitaxial, bond with the substrate, which does not involve a gradual relaxation of the elastic stresses as the film thickness increases.

According to the magnetization curves, ferrite-garnet films with a thickness of more than 100 nm, regardless of the composition of the buffer layer, are characterized by a saturation magnetization value close to that of the $Y_3Fe_5O_{12}$ single crystal, i.e. 1740 Gs and

a coercive force of 30 ... 40 O. This indicates that the films obtained are characterized by the stoichiometric composition of $Y_3Fe_5O_{12}$.

To determine the magnetic properties, measurements were made of the Kerr effect for films differing in buffer layers and thickness. In the polar configuration, the rotation of the Kerr angle θ_K for the $Y_3Fe_5O_{12}$(260nm)/AlO_x / SiO_x/S (100) heterostructure is 1530 degrees /cm (**Fig. 12***a*). It is known that in $Y_3Fe_5O_{12}$the contribution from Fe^{3+} ions in tetrahedral and octahedral sublattices has the opposite sign of the Faraday angle θ_F [42] and the resulting rotation θ_F at the incident light wavelength λ = 640 nm is 750 degrees/cm [35]. For a laser wavelength of 640 nm, the garnet ferrite film is optically transparent. Therefore, for submicron ferrite-garnet films, in the light reflection configuration, the Kerr rotation angle θ_K will be comparable to twice the angle of rotation of the polarization plane in a magnetic field θ_F $Y_3Fe_5O_{12}$ with a transparent thin buffer layer AlO_x. Accordingly, we can assume, taking into account the linear relationship between θ_F and saturation magnetization, that in this case the magnitude of the sublattice magnetization correspond to bulk ferrite garnet, and, therefore, the concentration of Fe^{3+} ions in tetrahedrons and octahedra is close to the stoichiometric composition of $Y_3Fe_5O_{12}$. For a ferrite garnet film on a relatively thick buffer layer of SiO_2, the angle $\theta_K \approx 820$ deg/cm is about 2 times smaller than for a sample with a buffer layer of AlO_x (Fig. 12*b*). Such a difference may be due to a relatively thick layer of SiO_2, which leads to an additional reflection of the incident beam of light at different interfaces, and the rotation of θ_K mainly occurs only in one direction - upon reflection from the Si (100) substrate.

In a magnetic field applied along the normal to the garnet surface, the films are characterized by a saturation field H_s of about 1.3 kOe (Fig. 12*a*), and in a field directed along the film plane, the value of the saturation field is about 0.06 kOe (Fig. 12*b*). Therefore, in these samples, the axis of easy magnetization is close in location to the film plane and determines the planar nature of the magnetic anisotropy. The coercive field in polycrystalline ferrite garnet films does not exceed 30 Oe and is typical of ferrite garnet films obtained on Si [43].

In **Fig. 13** shows the characteristic dependence of the amplitude of the FMR signal for ferrite-garnet films 260 nm thick on the external magnetic field and on the orientation of the samples, given by the polar θ_H and azimuthal φ_H angles. This makes it possible to measure the values of the resonant field and, according to the phenomenological model [44],

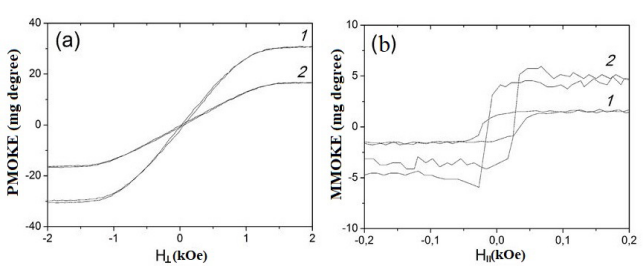

Fig. 12. *Field dependences of the polar (a) and meridional (b) Kerr effect for the characteristic $Y_3Fe_5O_{12}$(200nm)/AlO_x(40nm)/SiO_x (10nm)/Si (100) film heterostructures (Fig. 12a,b, curve 1) and $Y_3Fe_5O_{12}$(200nm)/SiO_2(800nm)/Si (111) (Fig. 12a,b, curve 2).*

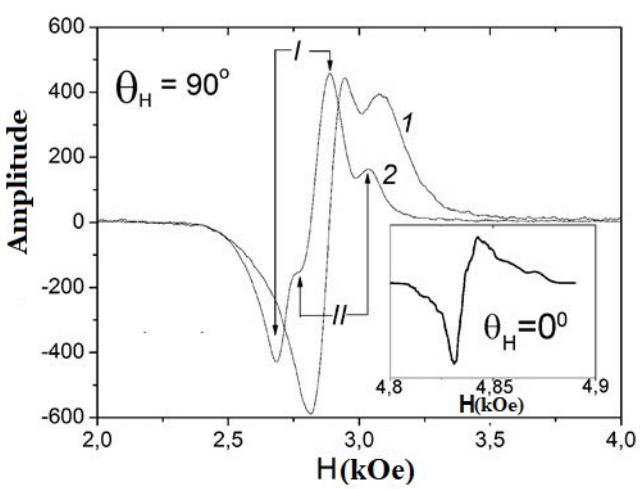

Fig. 13. *FMR spectra of characteristic $Y_3Fe_5O_{12}$(200nm)/ AlO_x(40nm)/SiO_x(10nm)/Si (100) film heterostructures (Fig. 13, curve 1) and $Y_3Fe_5O_{12}$(200nm)/SiO_2(800nm)/Si (111) (Fig. 13, curve 2) in a magnetic field oriented along the surface of the sample. The inset in Fig. 13 shows the FMR spectrum for sample $Y_3Fe_5O_{12}$(200nm)/SiO_2(800nm)/Si(111) in a magnetic field normally oriented to the sample surface.*

determine the values of the effective magnetic anisotropy constant K_{eff} for these samples, including the uniaxial anisotropy constant K_u and the demagnetization energy $2\pi M_S^2$. For the buffer layers under consideration, the value of Kerr was $-1 \cdot 10^5$ erg/cm^3. Note that the negative sign Kerr corresponds to the orientation of the axis of easy magnetization lying in the sample plane, and, therefore, correlates with the results obtained using the magneto-optical Kerr effect (Fig. 13).

From Fig. 13 that the FMR line for ferrite-garnet films, in the case of the direction of an external magnetic field along the sample plane, contains several resonances. This fact is the subject of a separate study. In the case of a garnet ferrite film on the AlO_x buffer layer, these resonances are difficult to distinguish. However, for a garnet ferrite film crystallized on a SiO_2 layer, the FMR line contains lines of two resonances, marked as I and II. The amplitude of the second resonance line decreases with a change in the direction of the external magnetic field from the plane of the sample surface to the normal to it. At $\theta_H = 0°$, only one contribution from the first resonance to the total signal is observed (inset to Fig. 13). Using the value for the width of the resonance curve ΔH, obtained for the resonant frequency of FMR, we can estimate the dimensionless damping parameter Hilbert α, which is determined by [35] from the relationship: $\Delta H \approx 2\pi f\alpha/\gamma$, where f is the FMR frequency, $\gamma = 1.7588 \cdot 10^7$ Oe^{-1} is the gyromagnetic ratio.

For samples with buffer layers in an external magnetic field applied parallel to the sample surface, the width of the first resonance line ΔH_1 is in the range of 150-200 Oe, while ΔH_2 is 270 O. However, for the perpendicular direction of the magnetic field ΔH_1 for ferrite films-granate on the AlO_x buffer layer is 150 Oe and 11 Oe for samples with a buffer layer of SiO_2 (inset to Fig. 13), which corresponds to the value of the Hilbert damping parameter $\alpha = 2.8 \cdot 10^{-3}$. The value of $\Delta H = 11$ Oe for the considered submicron films of ferrite-garnet, obtained by the method of ion-beam sputtering on silicon substrates, is 3-4 times higher than for films, by the method of pulsed laser evaporation PLD [44] and 3 times less than with films of ferrite garnets obtained by magnetron sputtering on GGG substrates [45].

The relaxation of spin-wave excitation processes in the samples under consideration is determined by their polycrystalline nature, the state of grain boundaries and the influence of the interface regions on the state of the film as a whole with its thickness specified by a limited range of values comparable to the value of 10 ... 100 lattice constants. In this case, in films of ferrite-garnet, inhomogeneous effective fields are created mainly due to the anisotropy of the crystal structure (random orientation of crystallites) and the anisotropy induced by stresses [46]. For the anisotropy field, Ha ~ $4\pi M_S$, and the width of the FMR line is determined by the expression $\Delta H = 0.5 H_a$ [35]. Since the field of uniaxial anisotropy is $H_U = 370$ Oe, an increase in the FMR line width in the structure of polycrystallites may be $\Delta H \approx 190$ O, which is in good agreement with the experimental value (Fig. 13). Due to the fact that $H_U \sim 4\pi M_S$, it should be expected that the interaction between the crystallites is weak, and the crystallites are resonantly excited in an external magnetic field independently of each other [35]. Therefore, the presence of two resonances in the FMR line (Fig. 13) may be due to two types of crystallites and intercrystallite boundaries differing in size (Fig. 13*a,b*), which are formed during deposition and subsequent crystallization. In addition, the value of the damping parameter is also affected by the buffer layer. It is known that a thermally oxidized SiO_2 layer on Si is

amorphous [46]. This provides a more stable structure of the SiO_2 layer, compared to the AlO_x layer obtained by precipitation at room temperature. Therefore, the ferrite-garnet film on the buffer layer of SiO_2 is less strained as compared to the film containing AlO_x. As a consequence, the ferrite-garnet film on the SiO_2 buffer layer in an external magnetic field perpendicular to the sample plane is characterized by a smaller contribution of randomly oriented crystallites to the total width of the FMR ΔH line.

The practical significance of applying the method of ion-beam sputtering to obtain submicron films of ferrite garnets on a SiO_2 buffer layer on silicon with the Hilbert decay parameter $\alpha \approx 10^{-3}$ is obvious. Film structures can be claimed in a large area of silicon spin-wave device structures.

6. CONCLUSION

A team of authors to create ferrite films on semiconductor substrates without elastic stresses and interactions of components at the interface created by crystallization of structures can give additional impetus for accelerated development of work in both spintronics and magnon-plasmon structures.

A distinctive feature of this method is that with its help it is possible to create structures not only of ferrites, but also of other film heterostructures with mismatched lattice parameters, group methods of microelectronics.

ACKNOLEDJMENTS

This work was supported by the RFBR projects No. 16-08-00933 and 16-29-05204.

REFERENCES

1. Zakharchenya BP, Korenev VL. Integrating magnetism into semiconductor electronics. UFN, 2005, 175 (6): 629-635 (in Russ.).
2. Joshi VK. Spintronics: A contemporary review of emerging electronics devices. *Engineering Science and Technology, an International Journal,* 2016, 19(3):1503-1513.
3. Nipan DG, Stogny AI, Ketsko VA. Oxide magnetic semiconductors: coatings and films. *Uspekhi khimii*, 2012, 5: 458-475 (in Russ.).
4. Sonoda S, Shimizu S, Sasaki T, Yamamoto Y. Molecular beam epitaxy of wurtzite (Ga, Mn)N films on sapphire(0001) showing the ferromagnetic behaviour at room temperature. *J. Cryst. Growth.*, 2002, 237:1358-1362.
5. Yang SG, Pakhomov AB, Hung ST, Wong CY. Room temperature magnetism in sputtered (Zn, Co)O films. *IEEE Transact. Magn.*, 2002, 38:2877.
6. Lim S-W, Hwang D-K, Myoung J-M. Observation of optical properties related to room-temperature ferromagnetism in co-sputtered $Zn_{1-x}Co_xO$ thin films. *Solid State Commun.*, 2003, 125:231-235.
7. Ramachandran S, Tiwari A, Narayan J. $Zn_{0.9}Co_{0.1}O$-based diluted magnetic semiconducting thin films. *Appl. Phys. Lett.*, 2004, 84:5255-5257.
8. Kim JH, Kim H, Kim D. Magnetic properties of epitaxially grown $Zn_{1-x}Co_xO$ thin films by pulsed laser deposition. *J. Appl. Phys.*, 2002, 92:6066-6071.
9. Lawes G, Risbud AS, Ramirez AP, Seshadri G. Absence of ferromagnetism in Co and Mg substituted polycrystalline ZnO. *Phys. Rev. B: Condens. Matter*, 2005, 71:045201-1-045201-5.
10. Kane MH, Salini K, Summers CJ. Magnetic properties of bulk $Zn_{1-x}Mn_xO$ and $Zn_{1-x}Co_xO$ single crystals. *J. Appl. Phys.*, 2005, 97:023906.
11. Mathias BT, Bozorth RM, van Vleck JH. Ferromagnetic Interaction in EuO. *Phys. Rev. Lett.*, 1961, 7(5):160-165.
12. Kumar D, Antifakos J, Blamire MG, Barber ZH. High Curie temperatures in ferromagnetic Cr-doped AlN thin films. *Appl. Phys. Lett.*, 2004, 84:5004-5006.
13. Ueda K, Tabata H, Kawai T. Magnetic and electric properties of transition-metal-doped ZnO films. *Appl. Phys. Lett.*, 2001, 79:988-1000.
14. Venkatesan M, Fitzgerald CB, Lunney JG, Coey JMD. Anisotropic Ferromagnetism in Substituted Zinc Oxide. *Phys. Rev. Lett.*, 2004, 93(17):7206-7209.
15. Sharma P, Gupta A, Rao KV. Ferromagnetism above room temperature in bulk and transparent thin films of Mn-doped ZnO. *Nat. Mater.*, 2003, 2:673-677.

16. Buchholz DB, Chang RPH, Song JH, Ketterson JB. Room-temperature ferromagnetism in Cu-doped ZnO thin films. *Appl. Phys. Lett.*, 2005, 87:1-082504-3.
17. Wang Z, Wang W, Tang J. Extraordinary Hall effect and ferromagnetism in Fe-doped reduced rutile. *Appl. Phys. Lett.*, 2003, 83:518-520.
18. Ogale SB, Choudhary RJ, Buban JP. High temperature ferromagnetism with a giant magnetic moment in transparent co-doped SnO(2-delta). *Phys. Rev. Lett.*, 2003, 91:077205-4.
19. Coey JMD, Douvalis AP, Fitzgerald CB, Venkatesan M. Ferromagnetism in Fe-doped SnO_2 thin films. *Appl. Phys. Lett.*, 2004, 84:1332-1334.
20. Hong NH, Sakai J, Prellier W, Hassini A. Transparent Cr-doped SnO_2 thin films: ferromagnetism beyond room temperature with a giant magnetic moment. *J. Phys.:Condens. Matter.*, 2005, 17:1697-1702.
21. Hong NH, Sakai J. Ferromagnetic V-doped SnO_2 thin. *Physica B.*, 2005, 358:265-268.
22. Wang CM, Jianga GeJ. Magnetic behavior of SnO_2 nanosheets at room temperature. *Appl. Phys. Lett.*, 2010, 97:42510.
23. Sundaresan A, Bhargavi R, Rangarajan N. Ferromagnetism as a universal feature of nanoparticles of the otherwise nonmagnetic oxides. *Phys. Rev. B.*, 2006, 74:161306-1-161306-4.
24. Mohanty S, Kar M, Ravi S. Ferromagnetism in mechanically milled pure SnO_2. *Intern. Journal of Modern Physics,* 2013, 27:1350025-1-1350025-11.
25. Nipan DG, Ketsko VA, Koltsova TN, Stogniy AI, Yanushkevich KI, Pankov VV, Khoviv AM. Solid solutions in the Zn-Co-O system: physicochemical properties. *Zh. Neorg Khimii*, 2006, 51 (12):2083-2089 (in Russ.).
26. Mathias BT, Bozorth RM, Vleck J.H. Ferromagnetic Interaction in EuO. *Phys. Rev. Lett.*, 1961, 7(5):160-165.
27. Appelbaum I, Huang B, Monsma DJ. Electronic measurement and control of spin transport in silicon. *Nature*, 2007, 447:295-299.
28. Schmehl A, Vaithyanathan V, Herrnberger A. Epitaxial integration of the highly spin-polarized ferromagnetic semiconductor EuO with silicon and GaN. *Nature Materials,* 2007, 6:882-887.
29. Ivanov V.A. Novotortsev VM, Kalinnikov VT. Spintronics and spintronic materials. *Izvestiya AN. Ser. Khimii*, 2004, 11:2255-2303 (in Russ.).
30. Randoshkin VV, Chervonenkis AY. *Prikladnaya magnitooptika.* Moscow, Energoatomizdat Publ., 1990, 320 p.
31. Mezin NI, Starostyuk NYu, Yampolskii SV. Growth and Properties of Yttrium Iron Garnet Films with a Higher Iron Content. *J. Magn. Magn. Mater.*, 2017, 442(15):189-195.
32. Popova Elena, Deb Marwan, Bocher Laura, Gloter Alexandre, Stéphan Odile, Warot-Fonrose Bénédict, Berini Bruno, Dumont Yves, Keller Niels. Interplay between epitaxial strain and low dimensionality effects in a ferromagnetic oxide. *Journal of Applied Physics,* 2017, 121:115304-1-115304-11.
33. Smirnova MN, Stogny AI, Bespalov AV, Golikova OL, Novitsky NN, Geraskin AA, Ermakov VA, Ketsko VA. The method of obtaining the heterostructure $Mg(Fe_{1-x}Ga_x)_2O_4/Si$ with a stable phase boundary. *Patent for IZ № 2657674*.
34. Beresnev EN, Smirnova MN, Goeva LV, Simonenko NP, Kopeva MA, Kuznetsova OB, Ketsko VA. Investigation of the process of decomposition of the gel and the formation of MgFe1.6Ga0.4O4 powder. *Zh. Neorg. Khimii,* 2016, 61 (8):1078-1083 (in Russ.).
35. Stogny AI, Novitsky NN, Golikova OL, Bespalov AV, Gieniusz R, Maziewski A, Stupakiewicz A, Smirnova MN, Ketsko VA. Formation by the method of ion-beam sputtering of submicron films of iron-yttrium garnet on silicon with buffer layers of silicon oxide or aluminum oxide. *Neorgan. Mater.*, 2017, 53 (10):1069-1074 (in Russ.).
36. Bhoi B, Venkataramani N, Aiyar RPRC, Prasad Sh. FMR and magnetic studies on polycrystalline YIG thin films deposited using pulsed laser. *IEEE Transactions on Magnetics*, 2013, 49(3):990-994.
37. Popova E, Keller N, Gendron F, Guyot M, Brianso MC, Dumond Y, Tessier M. Structure and magnetic properties of yttrium–iron–garnet thin films prepared by laser deposition. *J. Appl. Phys.*, 2001, 90(3):1422-1428.
38. Yang QH, Zhang HW, Wen QY, Liu YL. Effects of off-stechiometry and density on the magnetic and magneto-optical properties of yttrium iron

garnet films by magnetron sputtering method. *J. Appl. Phys.*, 2010, 108:073901-1-073901-5.

39. Boudiar T, Capraro S, Rouiller T, Blanc-Mignon MF, Payet-Gervy B, Berre MLe, Rousseau JJ. YIG thin films for magneto-optical and microwave applications. *Phys. Stat. Sol. (C),* 2004, 1(12):3347-3351.
40. International Centre for Diffraction Data. 1998, *JCPDS*. Card 43-0507.
41. Landolt-Börnstein. *Numerical Data and Functional Relationships in Science and Technology*. New Series. Group III. 27/e, 1991, Springer-Verlag, Berlin.
42. Zvezdin AK, Kotov VA. *Magnitooptika tonkikh plenok*. Moscow, Nauka Publ., 1988, 192 p.
43. Yang QH, Zhang HW, Wen QY, and Liu YL. Effects of off-stoichiometry and density on the magnetic and magneto-optical properties of yttrium iron garnet films by magnetron sputtering method. *J. Appl. Phys.*, 2010, 108:073901-1-073901-5.
44. Manuilov SA, Khartsev SI, Grishin AM. Pulsed laser deposited $Y_3Fe_5O_{12}$ films: Nature of magnetic anisotropy I. *J. Appl. Phys.*, 2009, 106:123917-1-123917-11.
45. Yamamoto S, Kuniki H, Kurisu H, Matsuura M, Jang P. Post-annealing effect of YIG ferrite thin-films epitaxially grown by reactive sputtering. *Phys. Stat. Sol. (A)*, 2004, 201(4):1810-1814.
46. Schlömann E. Inhomogeneous Broadening of Ferromagnetic Resonance Lines. *Phys. Rev.,* 1969, 182:632-645.